Scripta Materialia 144 (2018) 31–35

Contents lists available at ScienceDirect

Scripta Materialia

journal homepage: www.elsevier.com/locate/scriptamat

Regular Article

Effects of temperature on the irradiation responses of $Al_{0.1}CoCrFeNi$ high entropy alloy

Tengfei Yang [a,b], Songqin Xia [c], Wei Guo [d], Rong Hu [e], Jonathan D. Poplawsky [d], Gang Sha [e], Yuan Fang [a], Zhanfeng Yan [a], Chenxu Wang [a], Congyi Li [b], Yong Zhang [c], Steven J. Zinkle [b], Yugang Wang [a,*]

[a] State Key Laboratory of Nuclear Physics and Technology, Center for Applied Physics and Technology, Peking University, Beijing 100871, China
[b] Department of Nuclear Engineering, University of Tennessee, Knoxville, TN 37996, USA
[c] State Key Laboratory for Advanced Metals and Materials, University of Science and Technology Beijing, Beijing 100083, China
[d] Center for Nanophase Materials Sciences, Oak Ridge National Laboratory, Oak Ridge, TN 37831, USA
[e] Herbert Gleiter Institute of Nanoscience, Nanjing University of Science and Technology, Nanjing 210094, China

ARTICLE INFO

Article history:
Received 12 August 2017
Received in revised form 16 September 2017
Accepted 17 September 2017
Available online 29 September 2017

Keywords:
Irradiation effects
Structural damage
Chemical segregation
High-entropy alloy

ABSTRACT

Structural damage and chemical segregation in $Al_{0.1}CoCrFeNi$ high entropy alloy irradiated at elevated temperatures are studied using transmission electron microscopy (TEM) and atom probe tomography (APT). Irradiation-induced defects include dislocation loops, long dislocations and stacking-fault tetrahedra, but no voids can be observed. As irradiation temperature increases, defect density is decreased but defect size is increased, which is induced by increasing defect mobility. APT characterization reveals that ion irradiation at elevated temperatures can induce an enrichment of Ni and Co as well as a depletion of Fe and Cr at defect clusters, mainly including dislocation loops and long dislocations.

Published by Elsevier Ltd on behalf of Acta Materialia Inc.

High-entropy alloys (HEAs) are newly emerging advanced materials, which are defined as a multi-element solid solution composed of four or more principal elements in equimolar or near-equimolar ratios [1,2]. HEAs can exhibit high hardness, fatigue resistance, wear resistance and excellent low temperature fracture-resistance [3–6]. Specially, HEAs have a high softening resistance at elevated temperatures and sluggish diffusion kinetics. For these reasons, HEAs are widely regarded as promising high-temperature materials [7]. Due to their excellent mechanical properties and high temperature stability, HEAs have been proposed as structural materials in advanced nuclear systems [8,9], in which structural materials will be exposed to high temperatures and high irradiation doses.

Irradiation of alloys by energetic particles in nuclear reactors can cause serious structural damage, leading to the degradation of mechanical properties [10]. Therefore, the structural stability and mechanical properties of HEAs under irradiation are crucial for their applications in nuclear energy systems. Generally, irradiation-induced damage accumulation at room temperature is suppressed in HEAs [8], and the volume swelling induced by high temperature ion irradiation can be decreased by controlling the number and the type of alloying elements. As such, the volume swelling of FeCoCrMnNi HEA (<0.2%) is 30 times lower than that of Ni (~6.7%) under irradiation with 5 MeV Ni at 500 °C [11]. Although the irradiation response of HEAs has been studied, most of the experimental results are focused on the effects of compositional complexity on the irradiation resistance. The evolution of structural damage and chemical segregation with irradiation temperature in HEAs, which are important for a fundamental understanding of defect behavior and in determining the temperature range for its applications in nuclear system, have not been systematically studied.

In the current work, a single phase HEA $Al_{0.1}CoCrFeNi$ [12,13] is chosen as a model system to study the effects of temperature on the irradiation responses of HEA. The HEA $Al_{0.1}CoCrFeNi$ samples were irradiated by 3 MeV Au ions at 6×10^{15} cm^{-2} (~31 peak dpa); the irradiation temperatures ranged from 250 °C to 650 °C. Irradiation-induced defects and compositional segregation were characterized by transmission electron microscopy (TEM) and atom probe tomography (APT), respectively. Our aims are to investigate defect evolution and chemical segregation of HEA under high temperature irradiations, and provide reliable experimental results for obtaining a deeper understanding of the defect behavior in HEAs and the applications of HEAs in nuclear systems.

$Al_{0.1}CoCrFeNi$ HEA used in this study was synthesized by arc-melting a mixture of pure metals in a Ti-gettered high-purity argon atmosphere [12,14]. The polished samples were irradiated with 3 MeV Au ions at 250, 350, 500 and 650 °C, respectively. The details of ion irradiation can be found in Supplementary material. The corresponding displacements per atom (dpa) was calculated using SRIM 2013 assuming a displacement threshold energy of 40 eV in the Kinchin-Pease option [15].

* Corresponding author.
E-mail address: ygwang@pku.edu.cn (Y. Wang).

https://doi.org/10.1016/j.scriptamat.2017.09.025
1359-6462/Published by Elsevier Ltd on behalf of Acta Materialia Inc.

The irradiation fluences were 6×10^{15} cm^{-2}; the corresponding peak damage is ~31 dpa. The SRIM calculation results of dpa and Au distribution are given in Fig. S1 in Supplementary material. TEM observations were conducted using a 300 keV, Tecnai F30 microscope. Cross-sectional TEM samples were prepared by mechanical polishing, followed by ion milling to form a wedge for electron transparency. Irradiation-induced solute segregation in $Al_{0.1}$CoCrFeNi was characterized using APT (CAMECA LEAP 4000× HR or CAMECA LEAP 4000× SI) with a 50 pJ laser energy, a repetition rate of 200 kHz, and a specimen temperature of 30 K.

Fig. 1 shows the bright field (BF) images and corresponding selected area electron diffraction (SAED) patterns of $Al_{0.1}$CoCrFeNi HEAs irradiated at the four different temperatures. All BF images in Fig. 1 were taken under two-beam BF conditions using a diffraction vector $g = (0\bar{2}2)$ near the [211] zone axis and SAED patterns were taken under the [100] zone axis. No voids were observed at any of the four different sample temperatures. Furthermore, only diffraction spots belonging to a fcc structure can be found in selected area electron diffraction (SAED) patterns, indicating that no phase decomposition or incoherent precipitation occurs. At 250 °C (Fig. 1(a)), most of the visible irradiation-induced defects are located at the peak damage region (450 nm–650 nm). A high density of dislocation loops and small defect clusters, whose nature can't be distinguished, are observed. High-resolution TEM characterization in this depth region (as shown in Fig. 2(a)) revealed two groups of dislocation loops lying on the $(\bar{1}11)$ plane (indicated by red arrows) and $(1\bar{1}1)$ plane (indicated by blue arrows), suggesting that these small dislocation loops are faulted loops on the {111} plane. Fig. 2(b) presents the magnified HRTEM image of a dislocation loop in Fig. 2(a), which demonstrates that the dislocation loops are interstitial-type with $\boldsymbol{b} = 1/3\langle 111\rangle$. The average size of dislocation loops in this region was 7.4 ± 2.0 nm. A few large defect clusters including dislocation loops and dislocation line segments can be observed in the shallower region from 350 to 480 nm, but the densities are much lower.

As irradiation temperature increases to 350 °C (Fig. 1(b)), the depth-dependent microstructure is qualitatively similar to that at 250 °C. The region containing the highest density of small defect clusters and dislocation loops occurs over a somewhat narrower range of depths as compared with that of 250 °C, and the depth range of the region which consists of a low density of large dislocation loops and dislocation line segments is increased. This suggests that a portion of the small defects start to grow or become unstable and dissociate with increasing temperature, but the defect characteristics in both regions are overall similar with that of 250 °C.

Fig. 1(c) shows the BF image of $Al_{0.1}$CoCrFeNi irradiated at 500 °C, and it can be observed that the defect morphology and density are significantly different as compared with that of 250 °C and 350 °C. The defect density in the deeper region (510 nm–620 nm) is significantly decreased but the defect size is increased, with a greater number of easily resolvable isolated dislocation loops. A further microstructure characterization of this region (as shown in Fig. 2(c)) reveals that most of

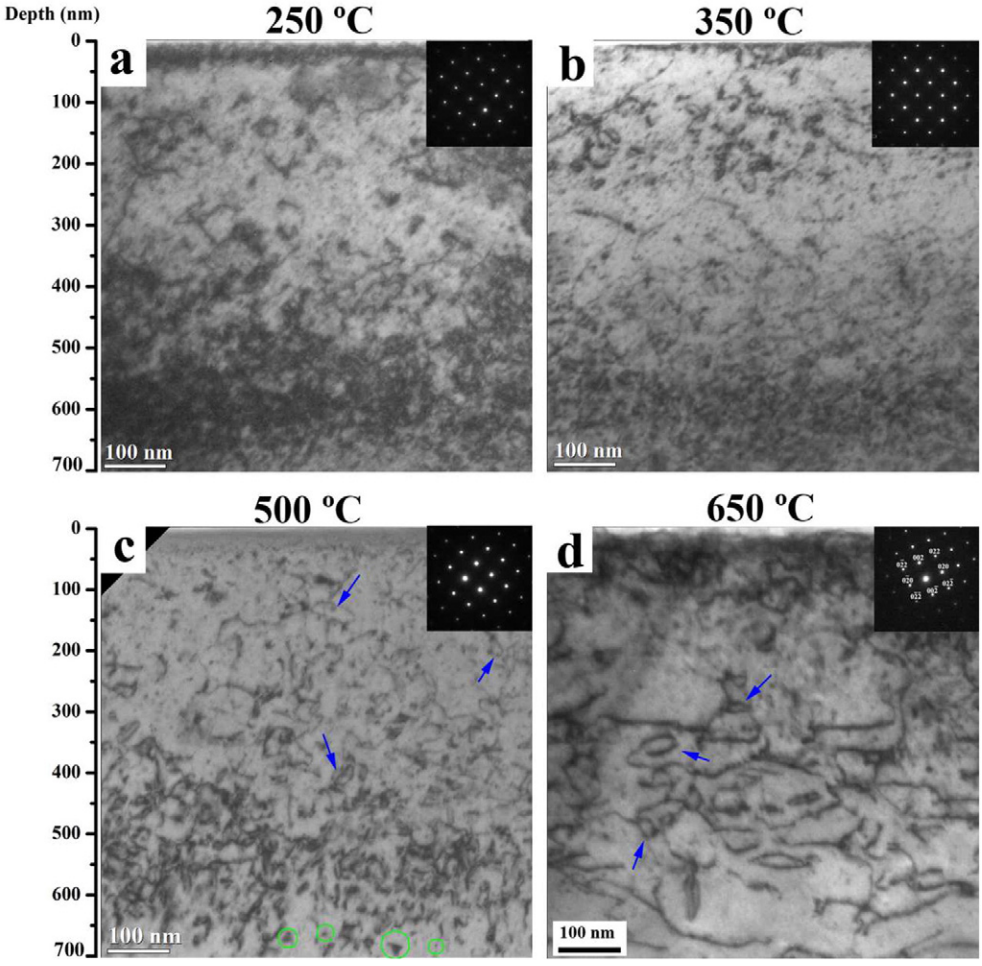

Fig. 1. BF images and corresponding SAED patterns of $Al_{0.1}$CoCrFeNi irradiated by 3 MeV Au ions to 6×10^{15} cm^{-2} at (a) 250 °C; (b) 350 °C; (c) 500 °C and (d) 650 °C, respectively. Perfect loops in (c) and (d) are marked by blue arrows and the green circles in (c) indicate SFTs.

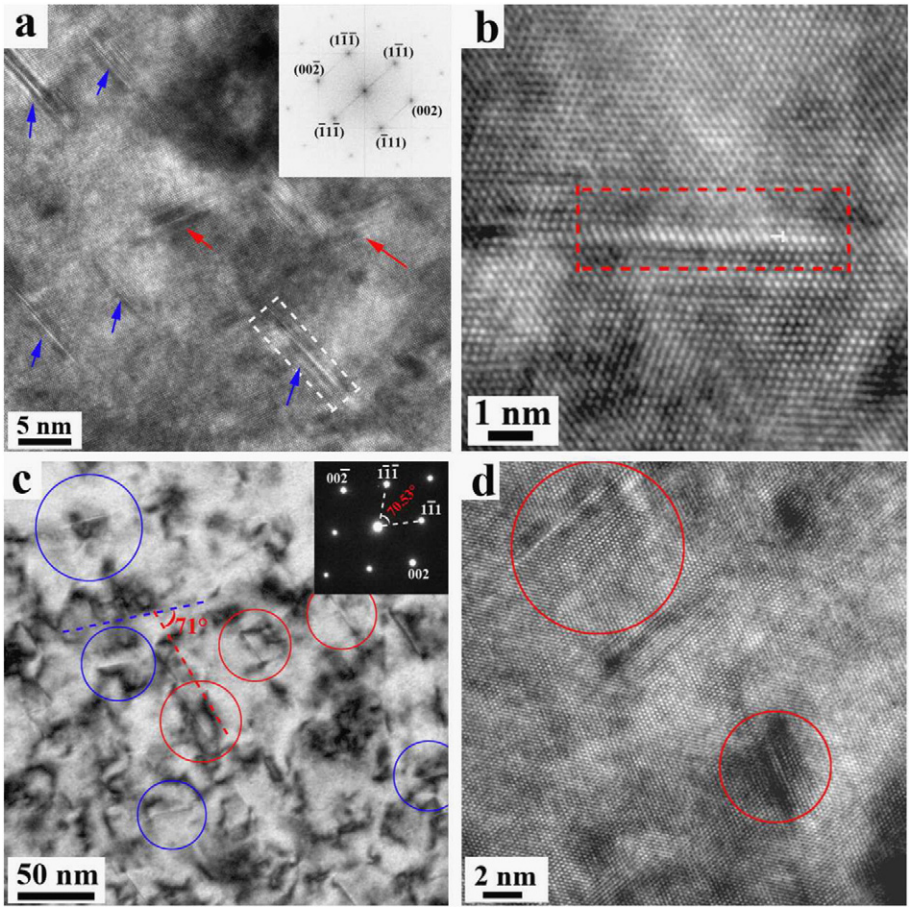

Fig. 2. (a) HRTEM images and corresponding FFT of $Al_{0.1}CoCrFeNi$ irradiated at 250 °C, the electron beam is along [110] zone axis; (b) Magnified HRTEM image of a dislocation loop formed at 250 °C (indicated by rectangle in (a)); (c) BF TEM image and corresponding SAED pattern of $Al_{0.1}CoCrFeNi$ irradiated at 500 °C. Two groups of edge-on faulted loops (indicated by red circles and blue circles, respectively) can be observed. (d) HRTEM image of SFTs (indicated by red circles) in $Al_{0.1}CoCrFeNi$ irradiated at 500 °C.

dislocation loops are also interstitial-type 1/3⟨111⟩ faulted loops, which is qualitatively similar with that of the lower temperature irradiations, but the average size increases to 35.2 ± 10.7 nm. A great number of stacking-fault tetrahedra (SFTs) can be also found in this region, as shown in Fig. 2(d). These SFTs are located at a deeper region, as compared with faulted loops, and appear as small black dots in low magnification BF images (as indicated by green circles in Fig. 1(c)). In the shallower region, numerous dislocations can be observed and this region further extends toward the surface, as compared with the irradiation temperature of 350 °C. An analysis using the invisibility criterion shows that the dislocations in this region have a Burgers vector 1/2 ⟨110⟩ . Besides the long dislocations, many perfect dislocation loops with $\boldsymbol{b} = 1/2\ \langle 110\rangle$ can be also observed (as indicated by blue arrows in Fig. 1(c)).

Fig. 1(d) shows the microstructure of $Al_{0.1}CoCrFeNi$ irradiated at the highest temperature 650 °C, where the density of irradiation-induced defects further decreases. Only long dislocation line segments and a low density of large perfect loops can be found. Faulted loops and SFTs are very infrequent, which indicates that the small defect clusters formed at low temperatures become thermally unstable at 650 °C and are readily annealed or absorbed by other defects.

To determine the phase stability and irradiation-induced compositional fluctuations, especially precipitation, APT characterizations were performed. Fig. 3 shows the 55 at.%_Ni + Co_iso-concentration surfaces (green surfaces) of $Al_{0.1}CoCrFeNi$ irradiated at different temperatures; the yellow color indicates the distribution of deposited Au ions. At first glance, the morphologies of Ni, Co-enriched clusters and their size and density variations with depth and irradiation temperature are consistent with that of irradiation-induced defects, which suggests that irradiation results in the segregation (solute enrichment) of Ni and Co preferentially at defects, such as dislocations loops and dislocation line segments. Irradiation-induced segregation at dislocations in the near surface region can be only observed at 500 and 650 °C, which is consistent with TEM observation that numerous long dislocation line segments are formed and extend toward the near surface region only at 500 and 650 °C. A great number of dislocation loops enriched with Ni and Co can be observed in the deeper regions (indicated by blue arrows). The dislocation loop size (as signified by the Ni + Co solute enriched region) evidently increases with irradiation temperature while the dislocation loop density is decreased. The quantitative variations of size and density of the Ni, Co-enriched dislocation loops as a function of temperature are given in Fig. S2 in Supplementary material. Since some small and irregular-shaped clusters in Fig. 3 are also included in the statistics, the measured dislocation loop sizes are smaller than the diameters of dislocation loops observed in TEM. At 250 and 350 °C, most Ni, Co-enriched dislocation loops are disk-shaped, indicating the segregation occurs on the whole habit plane of dislocation loops. However, a few ring-shaped dislocation loops can be also observed, as indicated within the red rectangles in Fig. 3(a) and (b). In these ring-shaped dislocation loops, the solute segregation only occurs at the edge of dislocation loops. As the temperature increases to 500 and 650 °C, all of the dislocation loops are disk-shaped.

Fig. 4 shows the proximity histograms of solute concentration profiles encompassing the matrix and dislocation loops for $Al_{0.1}CoCrFeNi$

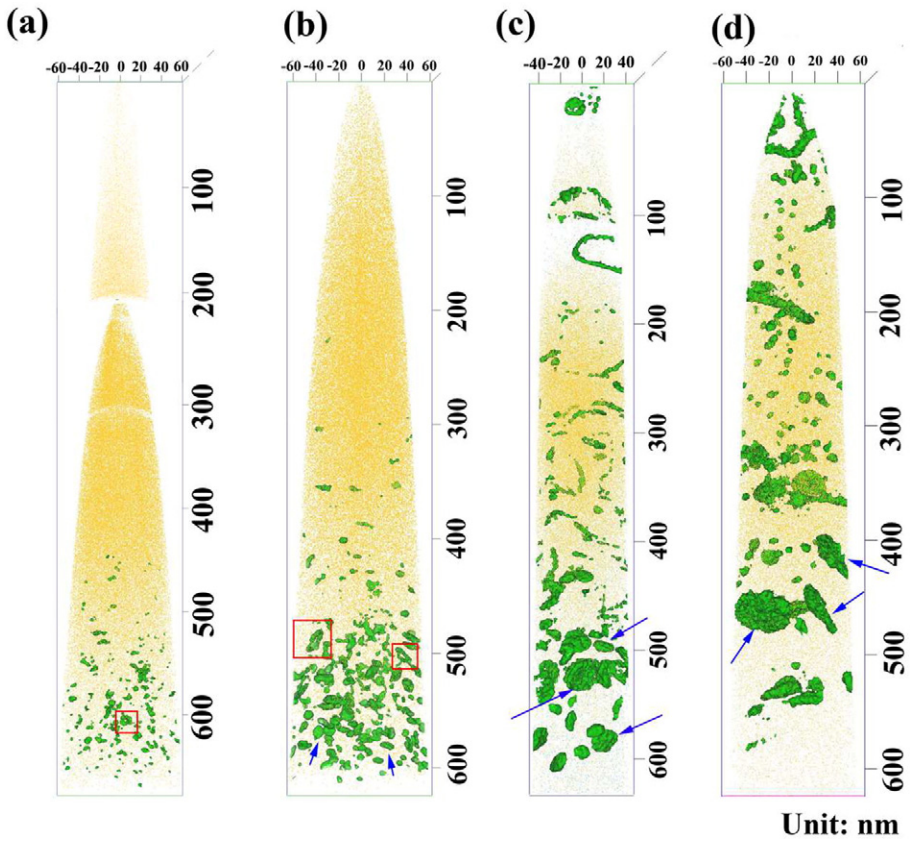

Fig. 3. 55 at.%_Ni + Co_iso-concentration surfaces of $Al_{0.1}CoCrFeNi$ irradiated at (a) 250 °C, (b) 350 °C, (c) 500 °C and (d) 650 °C. The deposited Au ions are indicated by yellow color. The blue arrows indicate the disk-shaped dislocation loops and the ring-shaped dislocation loops in (a) and (b) are marked by red rectangles.

irradiated at different temperatures, which verifies that Ni and Co tend to enrich, but Fe, Cr and Al deplete at the dislocation loops. The four different alloying elements vary by 30% to 60% between the matrix and dislocation loops. Co and Fe show slightly more segregation than the Ni and Cr, respectively, which is consistent with previous results in CoCrFeNi [16] and FeNiMnCr [17].

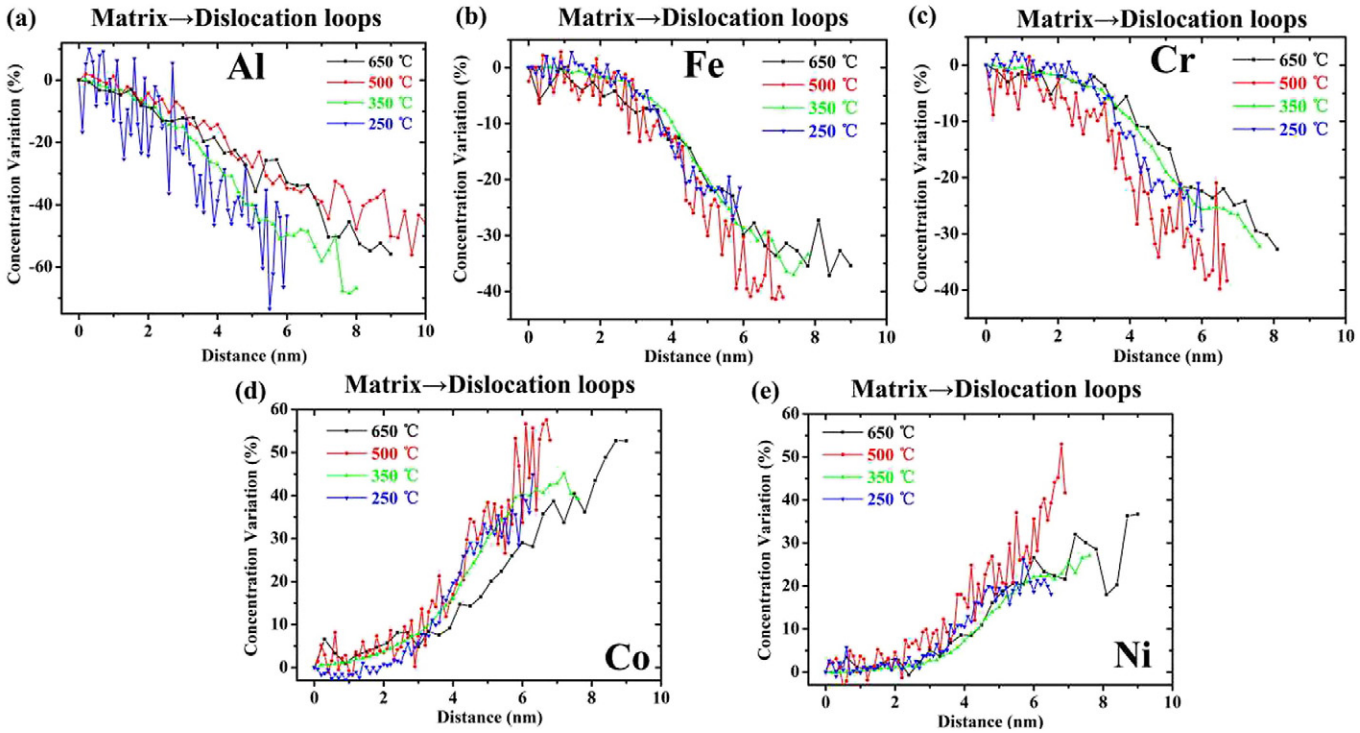

Fig. 4. Proximity histograms showing the variations in composition from matrix into dislocation loops for $Al_{0.1}CoCrFeNi$ irradiated at different temperatures.

TEM characterizations reveal that, as irradiation temperature increases, the defect density decreases and defect size increases. The irradiation-induced defects also transform from faulted loops and small defect clusters, whose nature cannot be distinguished, to perfect loops, SFTs and long dislocation line segments. The temperature-dependent irradiation-induced defect evolution in $Al_{0.1}$CoCrFeNi HEA is very similar with other fcc metals and alloys [18], and can be well interpreted by the defect mobilities and thermal stabilities [19]. At 250 °C, due to the low mobility, the migration and recombination of irradiation-induced defects are restrained, leading to the small defect size and high density. As temperature increases, the defect mobilities are enhanced, and simultaneously some small defect clusters become thermally unstable and can readily dissociate. The sizes of stable interstitial defects increase by absorbing the migrated interstitials, therefore, the defect density is decreased and defect sizes are increased with increasing temperature. At 250 °C and 350 °C, only interstitials and interstitial clusters have sufficient mobility to form visible dislocation loops and defect clusters, while the migration of vacancies is still restrained. As the irradiation temperature increases to 500 °C, vacancies become mobile and SFTs can be formed by the agglomeration of vacancies or in the displacement cascades. At the highest temperature 650 °C, small SFTs become thermally unstable, therefore the density of SFTs is greatly decreased. Faulted loops can transform into unfaulted (perfect) loops according to the known reaction (Eq. (1)), and long dislocations are formed due to loop unfaulting and coalescence [19].

$$1/3\langle 111\rangle + 1/6\langle 112\rangle = 1/2\langle 110\rangle \quad (1)$$

The APT characterization reveals that irradiation induced an enrichment of Ni and Co as well as a depletion of Fe, Cr and Al on dislocation loops and dislocations in $Al_{0.1}$CoCrFeNi in the temperatures range from 250 °C to 650 °C. Similar solute segregation behavior was also observed in other irradiated HEAs including CoCrFeNi (500 °C, 3 MeV Ni) [16] and FeCrMnNi (400–700 °C, 5.8 MeV Ni) [17]. Irradiation-induced enrichment of Ni and depletion of Cr at grain boundaries in 304L and 316L austenitic stainless steels, which is one of many factors that contribute to irradiation-induced stress corrosion cracking (IASCC), have been widely studied [20,21]. Similar segregation tendencies can be expected at dislocation loops and dislocations which also serve as sinks for irradiation-induced defects.

Generally, the irradiation-induced segregation behavior of major elements, such as Fe, Cr and Ni, at grain boundaries in austenitic stainless steels can be attributed to the inverse Kirkendall mechanism [22], in which the segregation behavior depends on the solute mobility. The defect sinks will be enriched with faster diffusing solutes and depleted in slower diffusing solutes, and the segregation behavior can be roughly determined by the relative atom sizes of solutes if the migration energies are unavailable. The undersized solutes (high mobility) tend to enrich, while oversized solute (low mobility) tend to deplete at defect sinks. For $Al_{0.1}$CoCrFeNi HEA, the corresponding atom radii are Fe-1.56 Å, Co-1.52 Å, Cr-1.66 Å and Ni-1.49 Å, respectively [23]. Therefore, undersized solutes Co and Ni enrich, and oversized solutes Fe and Cr deplete at these dislocation loops and dislocations.

In the current work, a representative HEA $Al_{0.1}$CoCrFeNi was irradiated by 3 MeV Au ions at four different temperatures to study the irradiation responses of HEA at elevated temperatures, including phase stability and evolutions of irradiation-induced defects and chemical segregation with temperature. It was found that $Al_{0.1}$CoCrFeNi exhibits great phase stability under high temperature ion irradiation; no significant phase transformation/decomposition can be observed. The defect density decreases but the defect size increases as increasing irradiation temperature, which is attributed to the enhanced defect mobility. Furthermore APT characterizations reveal that Ni and Co tend to enrich, but Cr and Fe prefer to deplete at dislocation loops and dislocations. Further calculations of atom diffusion in complex multi-component equiatomic alloys are required to quantitatively understand the irradiation-induced segregation behavior in HEAs.

Acknowledgements

This work was financially supported in part by the Office of Fusion Energy, U.S. Department of Energy (grant # DE-SC0006661), the National Magnetic Confinement Fusion Energy Research Project 2015GB113000 and the National Natural Science Foundation of China (11675005, 11335003, 91226202, 51471025 and 51671020), 111 Project (B07003), and the Program for Changjiang Scholars and the Innovative Research Team of the University. Part of the Atom probe tomography was conducted at ORNL's Center for Nanophase Materials Sciences (CNMS, Project NO. 2017-021), which is a U.S. DOE Office of Science User Facility. The authors acknowledge the use of facilities as well as scientific and technical assistance of the Materials Characterization Facility of Nanjing University of Science and Technology.

Appendix A. Supplementary data

Supplementary data to this article can be found online at https://doi.org/10.1016/j.scriptamat.2017.09.025.

References

[1] J.W. Yeh, S.K. Chen, S.J. Lin, J.Y. Gan, T.S. Chin, T.T. Shun, C.H. Tsau, S.Y. Chang, Adv. Eng. Mater. 6 (2004) 299–303.
[2] M.C. Troparevsky, J.R. Morris, M. Daene, Y. Wang, A.R. Lupini, G.M. Stocks, JOM 67 (2015) 2350–2363.
[3] P.K. Huang, J.W. Yeh, T.T. Shun, S.K. Chen, Adv. Eng. Mater. 6 (2004) 74–78.
[4] M.A. Hemphill, T. Yuan, G.Y. Wang, J.W. Yeh, C.W. Tsai, A. Chuang, P.K. Liaw, Acta Mater. 60 (2012) 5723–5734.
[5] M.-H. Chuang, M.-H. Tsai, W.-R. Wang, S.-J. Lin, J.-W. Yeh, Acta Mater. 59 (2011) 6308–6317.
[6] B. Gludovatz, A. Hohenwarter, D. Catoor, E.H. Chang, E.P. George, R.O. Ritchie, Science 345 (2014) 1153–1158.
[7] Y.P. Lu, Y. Dong, S. Guo, L. Jiang, H.J. Kang, T.M. Wang, B. Wen, Z.J. Wang, J.C. Jie, Z.Q. Cao, H.H. Ruan, T.J. Li, Sci Rep 4 (2014) 6200.
[8] D.S. Aidhy, C. Lu, K. Jin, H. Bei, Y. Zhang, L. Wang, W.J. Weber, Acta Mater. 99 (2015) 69–76.
[9] S.Q. Xia, X. Yang, T.F. Yang, S. Liu, Y. Zhang, JOM 67 (2015) 1–5.
[10] S.J. Zinkle, G. Was, Acta Mater. 61 (2013) 735–758.
[11] K. Jin, C. Lu, L.M. Wang, J. Qu, W.J. Weber, Y. Zhang, H. Bei, Scr. Mater. 119 (2016) 65–70.
[12] T. Yang, S. Xia, S. Liu, C. Wang, S. Liu, Y. Zhang, J. Xue, S. Yan, Y. Wang, Mater. Sci. Eng. A 648 (2015) 15–22.
[13] D. Li, C. Li, T. Feng, Y. Zhang, G. Sha, J.J. Lewandowski, P.K. Liaw, Y. Zhang, Acta Mater. 123 (2017) 285–294.
[14] T. Yang, S. Xia, S. Liu, C. Wang, S. Liu, Y. Fang, Y. Zhang, J. Xue, S. Yan, Y. Wang, Sci Rep 6 (2016) 32146.
[15] R.E. Stoller, M.B. Toloczko, G.S. Was, A.G. Certain, S. Dwaraknath, F.A. Garner, Nucl. Inst. Methods Phys. Res. B 310 (2013) 75–80.
[16] C. Lu, T. Yang, K. Jin, N. Gao, P. Xiu, Y. Zhang, F. Gao, H. Bei, W.J. Weber, K. Sun, Y. Dong, L. Wang, Acta Mater. 127 (2017) 98–107.
[17] N.A.P.K. Kumar, C. Li, K.J. Leonard, H. Bei, S.J. Zinkle, Acta Mater. 113 (2016) 230–244.
[18] M. Nastar, F. Soisson, Comprehensive Nuclear Materials. 1. Basic Aspects of Radiation Effects in Solids, ELSEVIER, Amsterdam, 2012.
[19] S. Zinkle, 1.03-radiation-induced Effects on Microstructure, Comprehensive Nuclear Materials, ELSEVIER, Amsterdam, 2012 65–98.
[20] Z. Jiao, G.S. Was, Acta Mater. 59 (2011) 1220–1238.
[21] Z. Jiao, G.S. Was, Acta Mater. 59 (2011) 4467–4481.
[22] T.R. Anthony, Acta Metall. 17 (1969) 603–609.
[23] E. Clementi, D. Raimondi, W. Reinhardt, J. Chem. Phys. 47 (1967) 1300–1307.